

# COMPARISON OF GAS PUFF IMAGING DATA IN NSTX WITH DEGAS 2 SIMULATIONS

B. CAO,<sup>a</sup> D. P. STOTLER,<sup>b\*</sup> S. J. ZWEBEN,<sup>b</sup> M. BELL,<sup>b</sup> A. DIALLO,<sup>b</sup> and B. LeBLANC<sup>b</sup>

<sup>a</sup>Chinese Academy of Sciences, Institute of Plasma Physics, Hefei 230031, China

<sup>b</sup>Princeton Plasma Physics Laboratory, P.O. Box 451, Princeton, New Jersey 08543

Received November 9, 2012

Accepted for Publication January 30, 2013

*Gas puff imaging is a two-dimensional diagnostic that measures the edge  $D_\alpha$  light emission from a neutral  $D_2$  gas puff near the outer midplane of the National Spherical Torus Experiment (NSTX). DEGAS 2 is a three-dimensional Monte Carlo code used to model neutral transport and plasma-neutral interactions in fusion plasmas. In this paper, we compare the measured and modeled  $D_\alpha$  light emission for specific NSTX experiments. Both the simulated spatial distribution and the radiance*

*of the  $D_\alpha$  light emission agree well with the experimental data obtained during time periods between edge-localized modes (ELMs) in ELMy H-modes.*

**KEYWORDS:** plasma diagnostics, neutral transport simulation, NSTX

*Note: The figures in this paper are in color only in the electronic version.*

## I. INTRODUCTION

Neutral deuterium plays an important role in tokamaks in that it typically provides the fuel for a discharge. However, deuterium atoms can also affect the energy balance of the plasma through radiation and charge exchange (e.g., see Ref. 1) and can, in theory, produce damping of ion toroidal momentum through charge-exchange collisions.<sup>2</sup> By being able to accurately measure neutral densities and model the behavior of neutral species, we can assess the magnitude of these effects as well as determine the efficiency of fueling sources.

The absolute value and radial profiles of the neutral deuterium density from recycling in the main chamber have been measured previously on several tokamaks. Measurements on the Texas Experimental Tokamak (TEXT) were made using a diagnostic neutral beam, a scanning neutral particle analyzer, and  $H_\alpha$  detectors to infer neutral deuterium densities that were  $\sim 10^{15} \text{ m}^{-3}$  in the plasma center and  $\sim 10^{17} \text{ m}^{-3}$  at the edge.<sup>3</sup> Measurements of edge neutral deuterium on Alcator C-Mod were made using Lyman alpha emission with inferred neutral densities in the range  $3 \times 10^{15}$  to  $3 \times 10^{17} \text{ m}^{-3}$  within  $\pm 3 \text{ cm}$  of the separatrix in an ohmic discharge.<sup>4</sup>

More recently, the spatial distribution of  $D_\alpha$  light emission was measured in Axially Symmetric Divertor Experiment (ASDEX) Upgrade using a calibrated camera, and neutral densities in the range  $0.5 \times 10^{16}$  to  $1 \times 10^{16} \text{ m}^{-3}$  were found near the separatrix.<sup>5</sup> No measurements of neutral deuterium density in the National Spherical Torus Experiment (NSTX) have been published, although an attempt was made to measure the neutrals using a camera with a  $D_\beta$  filter.<sup>1</sup> In Refs. 3, 4, and 5, to obtain the local neutral density it was necessary to use the plasma density and temperature profiles to interpret the line emission brightness and to reconstruct the local emission from the sight line line-averaged measurements.

We do not measure the recycling light in the present paper but instead measure the  $D_\alpha$  brightness of the deuterium light emission associated with the gas puff imaging (GPI) diagnostic on NSTX (Refs. 6, 7, and 8). This puff is similar to a fueling gas puff in that it is located at the outer midplane and puffs  $D_2$  gas at room temperature into the chamber during a plasma discharge. The  $D_\alpha$  light from the GPI gas puff is more than ten times larger than ambient  $D_\alpha$  emission due to other gas sources (see Sec. II) because those other gas sources (principally a center stack gas puff and recycling in the lower divertor) are at different locations and are not directly seen by the GPI optics. At the same time, the GPI gas puff is much smaller

\*E-mail: dstotler@pppl.gov

than those sources and does not noticeably impact the line-averaged density or edge-plasma parameters. For example, a typical average density in NSTX is  $5 \times 10^{19} \text{ m}^{-3}$  and the plasma volume is  $\sim 10 \text{ m}^{-3}$ , yielding a total content of  $5 \times 10^{20}$  electrons. The GPI gas puff represents  $\sim 3 \times 10^{20}$  deuterium atoms (see Sec. IV.B), but the DEGAS 2 simulations described here indicate that only  $\sim 20\%$  of these are ionized inside the separatrix so that the core source of electrons due to the puff is just  $6 \times 10^{19}$  electrons.

Interpretive analysis of existing divertor and edge experiments, as well as predictions of future ones (see, e.g., Ref. 9), rely heavily on coupled plasma-neutral transport codes because of the strong interactions between neutrals and plasma species in the vicinity of material surfaces where recycling occurs. Such interpretive simulations also frequently include, via the neutral transport codes, synthetic diagnostics that can simulate the signals from diagnostics based on the light emitted by neutral species. Those data are used to constrain the simulations and calibrate adjustable parameters. We can increase the confidence we have in the results of such applications by continuing to validate the neutral transport codes whenever an opportunity presents itself. The simulation of GPI experiments is a nearly ideal situation in that the source of the neutral species can be relatively well characterized, the plasma parameters in the vicinity of the light emission can be measured with reasonable accuracy, and the light emission can be recorded with fine spatial and temporal resolution.

The measured  $D_\alpha$  brightness from the GPI gas puff is compared here with DEGAS 2 neutral transport code<sup>10</sup> simulations. The initial study of GPI with DEGAS 2 was for deuterium in Alcator C-Mod (Ref. 11). That paper describes how the  $D_\alpha$  brightness was expected to vary with assumed spatial fluctuations in the local density and temperature and shows that excited atoms generated by molecular dissociation are a significant source of  $D_\alpha$  photons. A second paper describes DEGAS 2 modeling of helium GPI in NSTX (Ref. 12) and showed that the radial width of calculated He 587.6-nm brightness was in rough agreement with the GPI experimental results. That simulation also indicated that the finite extent of gas puff along the viewing direction did not significantly degrade the radial resolution of the diagnostic and provided a procedure to estimate the effective neutral density by comparing the simulation and the GPI experiment.

In a third paper on the analysis of GPI using DEGAS 2 (Ref. 13), the time response of the He 587.6-nm line emission to plasma density and temperature fluctuations is estimated to be  $\leq 1 \mu\text{s}$ , much less than a typical turbulence autocorrelation time of  $\sim 40 \mu\text{s}$  (Ref. 8). Consequently, the conventional atomic physics model, in which the effects of all excited atomic states are condensed into effective rate coefficients, is adequate for the interpretation of GPI experiments. Otherwise, one would need to explicitly simulate the time evolution of one or

more excited atomic physics states.<sup>13</sup> Reference 13 also showed that the calculated two-dimensional (2-D) spatial emission profiles of the He 587.6-nm line from DEGAS 2 matched well with the observed GPI in NSTX. Comparisons of the radial profiles of  $D_\alpha$  emission between GPI and DEGAS 2 are also presented for Alcator C-Mod in Ref. 7 and for He 587.6-nm emission for NSTX in Ref. 8.

The present validation effort is an advance over previous ones, first in that an absolute calibration has been obtained for the camera (the previous papers compared only profiles) and second in that the gas puff is deuterium (as opposed to helium). With regard to the latter, the physics of a  $D_2$  molecule can be vastly more complex than those of a helium atom. In fact, significant effort has been expended to incorporate the effects of excited molecular states (electronic, vibrational, and rotational) into Monte Carlo neutral transport codes<sup>14–16</sup>; these effects are expected to be significant in low-temperature, high-density divertor plasmas.<sup>14</sup> The validation tests described in this paper will show that the simpler model, ignoring excited molecular states, suffices for the higher temperatures and lower densities found in the NSTX scrape-off layer. Given the success of DEGAS 2 in modeling these GPI experiments, we plan to use related techniques to interpret passive light emission data, recorded by the diagnostic described in Ref. 1, to not only infer neutral density profiles but to learn more about neutral sources in the main chamber of NSTX.

We will describe the GPI diagnostic and its calibration in Sec. II. The DEGAS 2 neutral transport code is introduced in Sec. III along with a simpler kinetic neutral transport code, KN1D. Our results are presented in Sec. IV, in comparison first of 2-D profiles and then of the absolute magnitude of the light emission. Finally, our findings are summarized in Sec. V.

## II. GPI DIAGNOSTIC IN NSTX

A brief review of the GPI diagnostic on NSTX is included here; more details can be found in Refs. 6, 7, and 8. The GPI measurement on NSTX is a 2-D diagnostic of edge turbulence near the outer midplane. A gas-puffing manifold with 30 holes of 1-mm diameter and 1 cm apart located at the outer wall behind the projection of the radio-frequency (rf) antenna introduces a deuterium gas puff into the plasma; the visible line emission from this gas cloud is then imaged by a fast camera. Since the turbulence is highly elongated along the magnetic field, the  $D_\alpha$  light from the GPI gas puff cloud is viewed along the local magnetic field to resolve the smaller-scale radial versus the poloidal structure of the turbulence.

Figure 1a is a schematic of the GPI gas puff cloud and the camera view along the magnetic field, and Fig. 1b

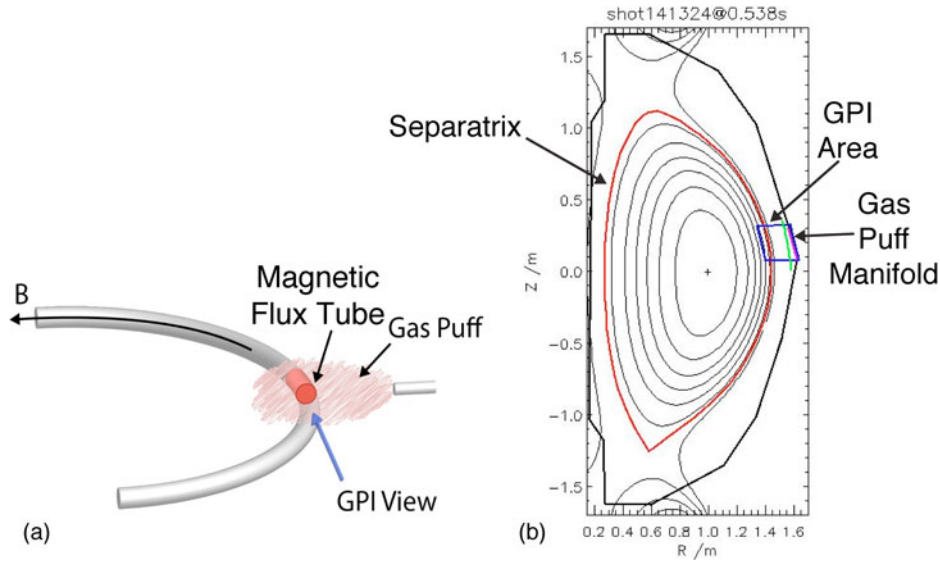


Fig. 1. (a) Schematic of the GPI diagnostic geometry and (b) location of GPI diagnostic in NSTX. The GPI fast camera views the  $D_\alpha$  light emitted from the gas puff cloud along the local magnetic field direction. The separatrix (without the X-point), GPI viewing area, and gas puff manifold are indicated.

shows the location of the GPI view, which is near the separatrix and  $\sim 20$  cm above the midplane. The fast camera used on NSTX for this experiment took images at 397 660 frames per second, and the resolution of the optics was  $64 \times 80$  pixels. The exposure time was  $\Delta t_i = 2.1 \mu\text{s}$ . This camera imaged the  $D_\alpha$  light from the gas cloud through a  $657 \pm 5$  nm filter [full-width at half-maximum (FWHM)]. The GPI gas puff increased the brightness of the  $D_\alpha$  by approximately 20 times above the background and thus localized the emission for improved spatial resolution. The spatial resolution of the optics is  $\sim 0.3$  cm at the gas cloud.

We have performed an absolute optical calibration of the GPI camera with the objective of determining the number of  $D_\alpha$  photons emitted per injected D atom. Since only the total number of D atoms injected by the GPI gas puff is known, and not the instantaneous flow rate, this will be the basis used for comparison with the DEGAS 2 simulations. The experimental calibration was made with a white-light calibration lamp,<sup>a</sup> which had a spectral radiance at 650 nm (near  $D_\alpha$ ) of  $1.02 \times 10^{-7}$  W/sr $\cdot$ cm $^2$  $\cdot$ nm. The entire GPI optical system including the front-end mirror and lenses, fiber bundle,  $D_\alpha$  filter, and camera (except for the vacuum window) was removed from NSTX and set up to view this calibration lamp. Since the  $D_\alpha$  filter had a calibrated FWHM of  $\sim 10 \pm 1$  nm, the radiance of this lamp as viewed by the GPI optics was  $1.02 \times 10^{-6} \pm 15\%$  W/sr $\cdot$ cm $^2$ .

One pixel in the center of the image of the lamp had a time-averaged camera signal of  $639 \pm 5\%$  counts for an

exposure time of 41 000  $\mu\text{s}$ . Thus, the absolute response of the camera to this source of  $D_\alpha$  light was  $1.56 \times 10^{-2}$  count/ $\mu\text{s}$  per pixel for a source of  $1.02 \times 10^{-6}$  W/sr $\cdot$ cm $^2$ . Since each  $D_\alpha$  photon has an energy of 1.9 eV, this implies that 1 count/ $\mu\text{s}$  per pixel corresponds to  $2.16 \times 10^{14}$  photons/(sr $\cdot$ cm $^2$  $\cdot$ s). The vacuum window transmission was measured to be 0.88 after the run so that the absolute response of the camera to the  $D_\alpha$  light source is 1 count/ $\mu\text{s}$  per pixel for  $\beta = 2.45 \times 10^{14}$  photons/(sr $\cdot$ cm $^2$  $\cdot$ s). Again, this calibration was performed with a single pixel; a separate relative calibration showed a sensitivity variation of  $\pm 10\%$  across the image, yielding a total uncertainty in the calibration factor of  $\pm 19\%$ . Because this relative calibration was performed ex situ, the camera view differed from that used in the GPI experiments. Otherwise, we could directly account for the sensitivity variations by factoring the resulting data into the simulated images. Note, however, that this calibration is independent of the distance of the source from the camera since the calibration pixel was chosen to be in the center of the lamp window and since radiance is independent of the distance from the source to the lamp.

### III. DEGAS 2 AND KN1D NEUTRAL TRANSPORT CODES

DEGAS 2 simulates the transport of neutrals through plasma and vacuum using the Monte Carlo method.<sup>10–13</sup> In these particular simulations, the 30 holes of the GPI gas manifold are represented as ten  $2 \times 2$ -cm squares aligned with the pitch of the actual manifold. The simulations are run in steady state with a specified, but arbitrary,

<sup>a</sup>Optronic Laboratories Model 420.

gas puff rate. The deuterium molecules are sampled randomly from a 300 K thermal energy and cosine angular distributions. As the molecules penetrate the plasma, they undergo ionization, dissociation, and elastic scattering; resulting molecular ions are assumed to be ionized, dissociated, or recombined immediately. Any product atoms are then tracked through the plasma and interact with it via ionization and charge exchange.<sup>11</sup> The particle track terminates upon ionization of the atom. Along the particles' paths, the volumetric source of  $D_\alpha$  photons is accumulated in each computational zone.

The emission rate of that  $D_\alpha$  light is computed by an expression equivalent to

$$S_{D_\alpha} = \sum_{j=D, D_2, D_2^+} n_j f_j(n_e, T_e), \quad (1)$$

where

$n_j$  = computed density of the electronic ground-state atom, molecule, or molecular ion

$n_e$  = electron density

$T_e$  = electron temperature.

The function  $f_D$  is the ratio of the density of the upper level of the radiative transition to the ground-state density times the rate of spontaneous decay (Einstein coefficient) for the transition; the  $D_\alpha$  line results from a principal quantum number  $n = 3 \rightarrow 2$  transition. The local distribution of neutral atoms over the electronically excited states is obtained from a collisional radiative model (see, for example, Ref. 17) based on that described in Ref. 18 and utilizing the cross sections of Ref. 19. The emission associated with  $D_2$  and  $D_2^+$ , responsible for  $\sim 30\%$  of the total, is computed using the expressions in Ref. 11. As noted in Sec. I, this model for the molecules is relatively simple compared with more recent ones.<sup>14–16</sup>

The principal output of the DEGAS 2 calculations is the simulated view of the GPI camera obtained by integrating through the simulation volume along a chord corresponding to each of the  $80 \times 64$  pixels.

The experimental data from a particular shot and time required to define the input parameters for DEGAS 2 are the magnetic equilibrium, computed with EFIT (Refs. 20 and 21), and the radial electron density and temperature profiles, obtained from the Thomson scattering diagnostic on NSTX as a function of major radius at midplane. The DEGAS 2 geometry is constructed using contours of constant poloidal magnetic flux drawn inside a toroidally axisymmetric rectangle encompassing the emission volume viewed by the GPI camera. The plasma densities and temperatures (with  $n_i = n_e$  and  $T_i = T_e$ ) are mapped onto these contours as a function of major radius and are assumed to be constant along the contours over the spatial extent of this box. With this approach, the role of the EFIT equilibrium is only to determine the shapes

of the flux surfaces, which do not vary dramatically; the less-well-determined location of the separatrix does not enter. For the baseline simulations, the radial spacing of the contours is  $\sim 0.5$  cm inside the separatrix (where the plasma gradients are steep) and  $\sim 1$  cm outside. The points along each contour are separated by  $\sim 1$  cm. The fundamental geometric elements in a particular toroidal plane are triangles drawn between adjacent points on adjacent contours. These are translated into volumes by rotation through a specified range of toroidal angle (0.6 deg in the vicinity of the emitting volume). A sensitivity study done with three times as many contours yields a simulated camera image indistinguishable from the baseline and an integrated photon count differing by  $< 1\%$ . Another sensitivity test performed with the vertical extent of the rectangle increased by 50% again results in an image indistinguishable from that of the baseline; the integrated photon count increased by only 3%.

For comparison, we also used the KN1D code<sup>22</sup> to calculate one-dimensional (1-D) radial neutral density profiles and the corresponding  $D_\alpha$  light emission due to deuterium gas coming from the wall (e.g., due to recycling and outgassing) and not specifically from a GPI gas puff. KN1D is a kinetic transport code for simulating the penetration of atomic and molecular hydrogen into a ionizing plasma, utilizing one spatial and two velocity dimensions. The NSTX Thomson scattering data for the electron density and temperature profiles are input to KN1D assuming that the ions and electrons have the same temperature. KN1D runs using the same  $T_e$ , but different  $T_i$  show no significant differences. For the neutral transport to effectively be 1-D in space, one needs a neutral source with spatial dimensions much larger than the penetration depth; this approximation is questionable for the GPI problem. On the other hand, the input for KN1D is relatively easy to set up, and the code runs quickly, facilitating parameter scans.

## IV. COMPARISON OF DEGAS 2 AND GPI

### IV.A. Profile Comparison

In this section we will present the measured 2-D profiles of the time-averaged  $D_\alpha$  light emission from the GPI gas puff and compare them with those obtained with the neutral transport simulation code DEGAS 2. Section IV.B will describe the absolute calibration.

For this comparison we use four shots (also used in Ref. 23) taken on the same NSTX run day, as listed in Table I. All of these shots are H-mode discharges with considerable lithium coating, a toroidal magnetic field 4.3 kG, and a plasma current of 650 to 700 kA. The total size of the  $D_2$  GPI gas puff was nominally the same for all shots and measured to be  $5.3 \pm 0.1$  Torr· $\ell$  ( $\sim 1.7 \times 10^{20}$  molecules) via the drop in plenum pressure before and after the puff.

TABLE I

Shot List, Plasma Parameters, and Comparison Between GPI and DEGAS 2

Shot	Start Time (ms)	$P_{NBI}$ (MW)	$n_e$ ( $10^{13} \text{ cm}^{-3}$ )	$I_p$ (kA)	$B$ (kG)	Total Gas Puff (Torr· $\ell$ )	GPI–DEGAS 2 Peak Difference (cm)	GPI–DEGAS 2 Width Difference (cm)	GPI–DEGAS 2 Intensity Ratio
#141307	480	3.8	7.5	700	4.43	5.2	0.4	0.8	0.90
#141320	530	4.0	8.0	650	4.43	5.3	0.4	2.1	0.79
#141322	530	4.0	8.0	650	4.43	5.4	1.0	0.9	0.93
#141324	530	2.9	6.0	650	4.43	5.3	0.4	0.2	1.00

The time evolution of the mean  $D_\alpha$  light signal from this GPI gas puff for the four shots is shown by the bottom curves of Fig. 2. These curves come from averaging the total number of counts in each GPI camera frame over all pixels. The gas is puffed into the steady-state part of the discharge at  $\sim 0.5$  s; the  $D_\alpha$  light from the puff is visible starting  $\sim 15$  ms after the onset of the gas puff. The gas puff light peaks  $\sim 30$  ms after it starts and then decays with a time constant of  $\sim 50$  ms as the gas is exhausted from the manifold. Using the calibration factor  $\beta$  from Sec. II and the exposure time  $\Delta t_i$ , we see that

a mean intensity of 100 corresponds to  $1.17 \times 10^{16}$  photons/(s·sr·cm<sup>2</sup>). The peak value of the mean GPI intensity is about the same for all shots, as is expected from the similar gas puff levels. Also shown in Fig. 2 are the outer midplane separatrix position versus time and the location of the radial peak of the GPI light, which are discussed at the end of this section.

The time periods used for comparing GPI and DEGAS 2 profiles are shown by the gray-shaded regions in Fig. 2. These are all 10-ms intervals near the peak of the GPI signal during which time there are no

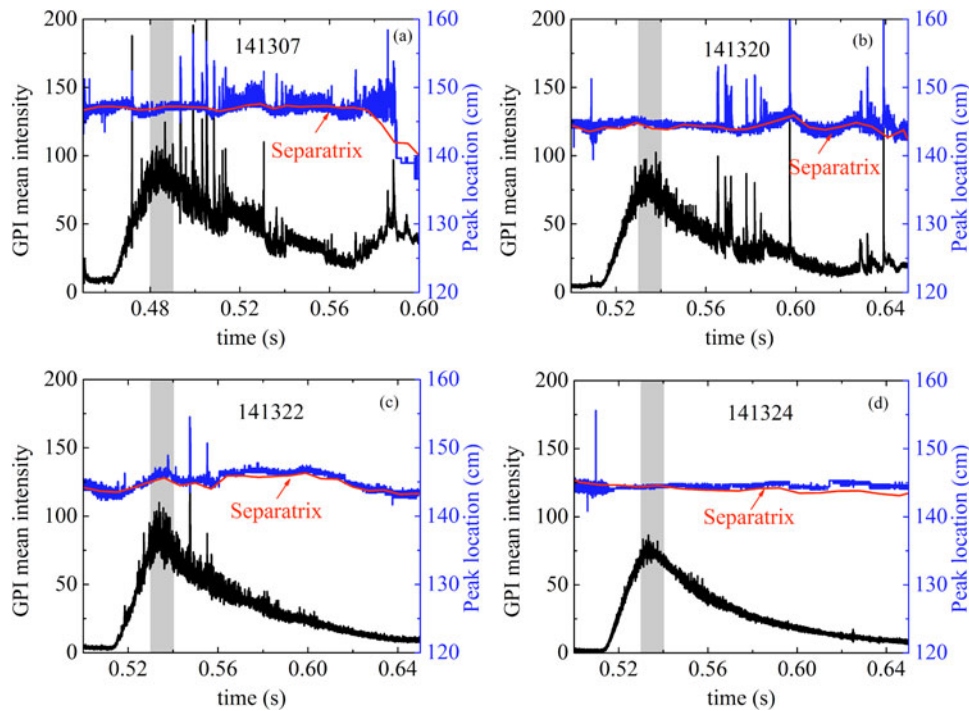


Fig. 2. Time dependence of mean GPI intensity (left axis and bottom trace in each frame) and peak location (right axis and top trace) mapped to the outer midplane. The GPI puff begins to be visible  $\sim 15$  ms after the start of these traces. The gray areas are the time regions used in this paper. The separatrix location (right axis and narrow line indicated by arrow) at the outer midplane is also shown. As is described in the text, a GPI mean intensity of 100 corresponds to  $1.17 \times 10^{16}$  photons/(s·sr·cm<sup>2</sup>).

edge-localized modes (ELMs) (the large spikes occurring later in shots #141307 and #141320). Note that a nominal frequency for type III ELMs in NSTX is 460 Hz (Ref. 24). The Thomson scattering electron density and temperature data taken at these times are shown in Fig. 3.

Figures 4 through 7 show the 2-D comparisons of the  $D_\alpha$  light emission from the GPI data with the  $D_\alpha$  emission calculated from the DEGAS 2 simulations of the shots in Table I. In Figs. 4a, 5a, 6a, and 7a, the color contours are from the simulation (color online), with units of  $W/(sr \cdot m^2)$ , and in white are equally spaced contours for the 2-D GPI  $D_\alpha$  emission profiles averaged over the 10-ms periods shown in Fig. 2. In Figs. 4 through 7, the local radial coordinate is approximately horizontal, the local poloidal coordinate is approximately vertical, the separatrix is shown by the black dashed line, the limiter (downstream rf antenna) is shown by the rightmost dashed line, and the GPI gas manifold location is shown by the nearly vertical line.

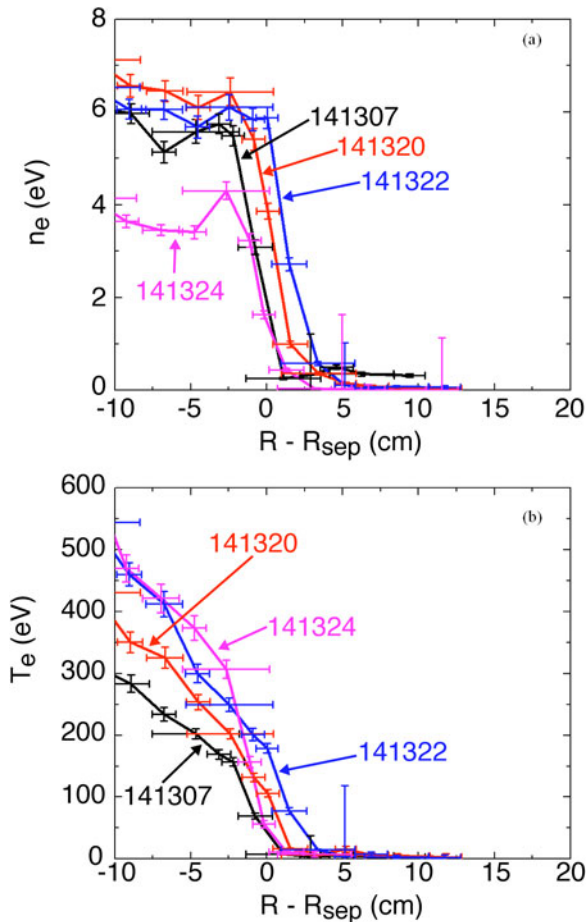


Fig. 3. Radial profiles from the Thomson scattering diagnostic for (a) the electron density and (b) the electron temperature relative to the separatrix location for the shots and times in Table I. The GPI field of view is typically in the vicinity of the separatrix.

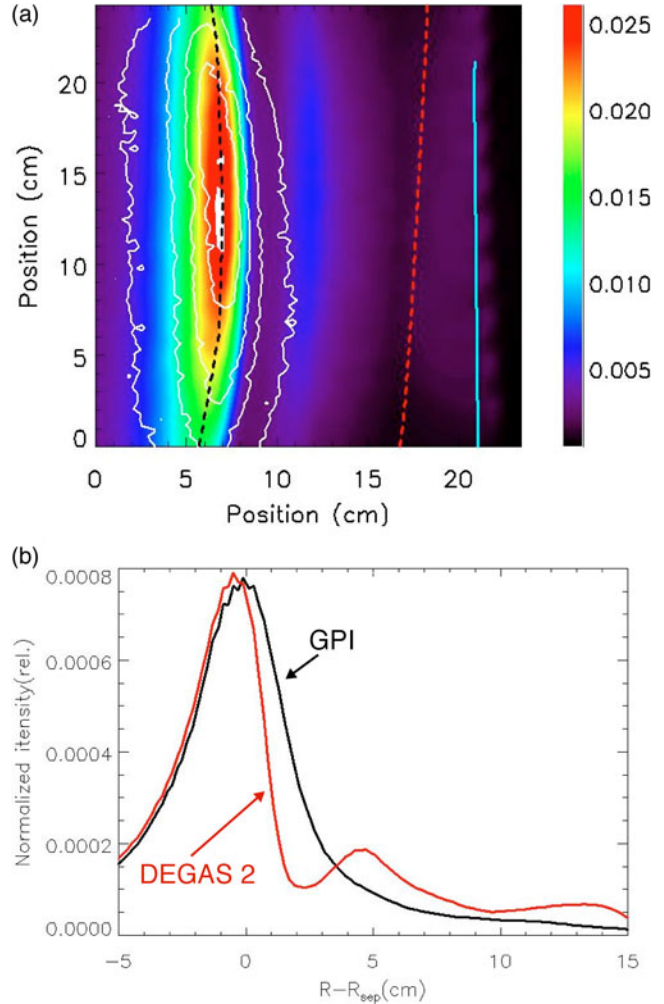


Fig. 4. Comparison between the  $D_\alpha$  light emission from DEGAS 2 and GPI data for #141307. (a) The color contours are the DEGAS 2 results in units of  $W/(sr \cdot m^2)$  (for a gas puff rate of  $8.2 \times 10^{17}$  D atoms per second), the equally spaced white contours are the GPI results, the leftmost dashed line is the separatrix, the rightmost dashed line is the limiter shadow, and the nearly vertical line is the gas manifold. (b) The 1-D profiles are obtained by normalizing the 2-D data to the sum over all pixels and then averaging over vertical pixels. The horizontal coordinate is mapped to the outer midplane separatrix.

Figures 4b, 5b, 6b, and 7b show the relative shapes of the radial distributions of the  $D_\alpha$  light emission from both GPI and DEGAS 2. These are found by normalizing the 2-D data to the sum over all pixels, averaging the result over vertical pixels, and then mapping the horizontal coordinate to the major radius at the midplane relative to the separatrix. The differences between the locations of the peaks in the radial profiles of GPI and DEGAS 2 are listed in Table I; the differences between these peak locations vary between 0.4 and 1.0 cm. Also

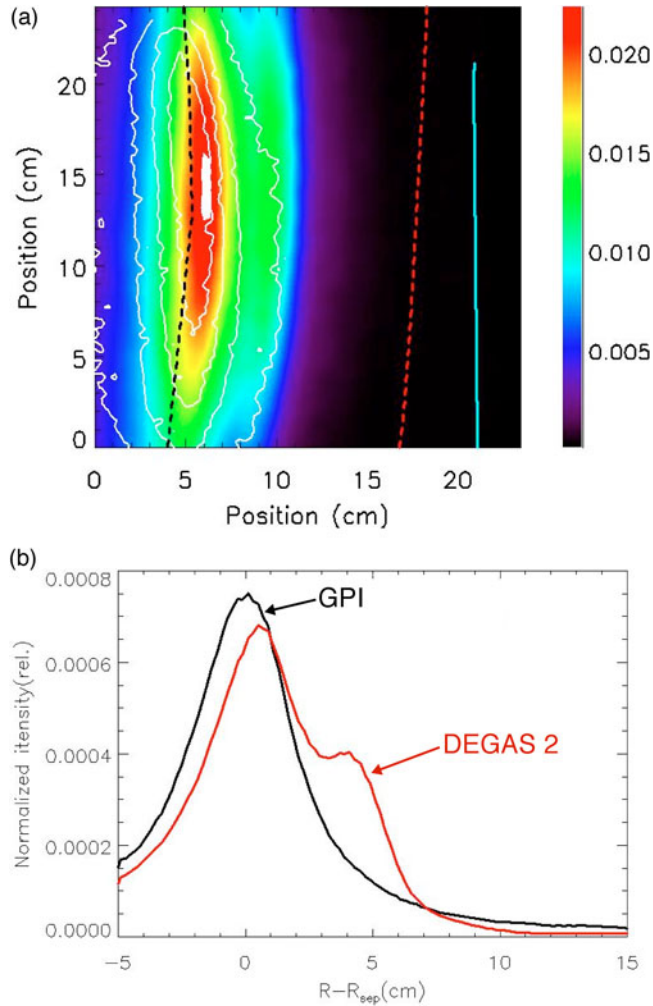


Fig. 5. Comparison between the  $D_\alpha$  light emission from DEGAS 2 and GPI data for #141320. (a) The color contours are the DEGAS 2 results in units of  $W/(sr \cdot m^2)$  (for a gas puff rate of  $8.2 \times 10^{17}$  D atoms per second), the equally spaced white contours are the GPI results, the leftmost dashed line is the separatrix, the rightmost dashed line is the limiter shadow, and the nearly vertical line is the gas manifold. (b) The 1-D profiles are obtained by normalizing the 2-D data to the sum over all pixels and then averaging over vertical pixels. The horizontal coordinate is mapped to the outer midplane separatrix.

listed in Table I are the differences in the radial widths (FWHM) of these distributions for each shot; these range from 0.2 to 2.1 cm. For reference, the widths of the GPI emission profiles vary between 4.2 and 4.7 cm. The uncertainties in both the simulated and experimental profile peaks and widths are roughly  $\pm 1$  pixel (Ref. 13), i.e.,  $\pm 0.3$  cm. Thus, the relative shapes of 2-D emission profiles for  $D_\alpha$  from DEGAS 2 and GPI results match in most cases to within these uncertainties, as was the case for the earlier analyses of helium GPI in NSTX (Ref. 13).

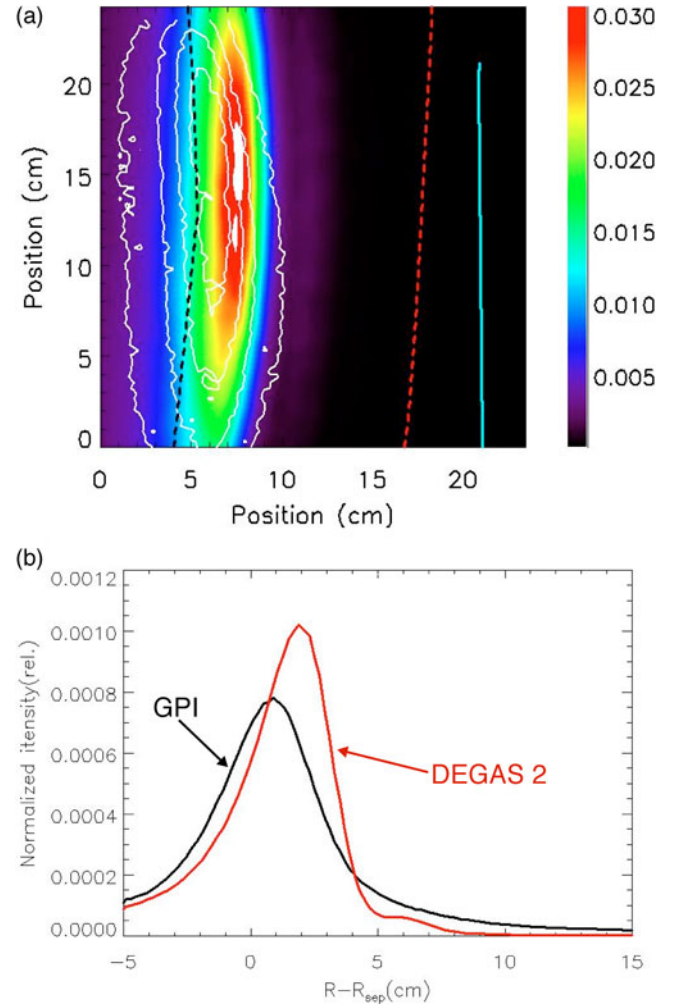


Fig. 6. Comparison between the  $D_\alpha$  light emission from DEGAS 2 and GPI data for #141322. (a) The color contours are the DEGAS 2 results in units of  $W/(sr \cdot m^2)$  (for a gas puff rate of  $8.2 \times 10^{17}$  D atoms per second), the equally spaced white contours are the GPI results, the leftmost dashed line is the separatrix, the rightmost dashed line is the limiter shadow, and the nearly vertical line is the gas manifold. (b) The 1-D profiles are obtained by normalizing the 2-D data to the sum over all pixels and then averaging over vertical pixels. The horizontal coordinate is mapped to the outer midplane separatrix.

Also shown in Table I are the ratios of the measured GPI light to the DEGAS 2 predicted  $D_\alpha$  light within this field of view for the 10-ms period of interest for each shot, normalized so that this ratio is assumed to be 1.00 for #141324. These are all within 0.79 to 1.0, indicating that the ratio of the GPI/DEGAS 2 light intensity is fairly consistent from shot to shot in this database.

The small differences between the observed and calculated  $D_\alpha$  profiles of Figs. 4 through 7 can be attributed to uncertainties in the assumed density and electron

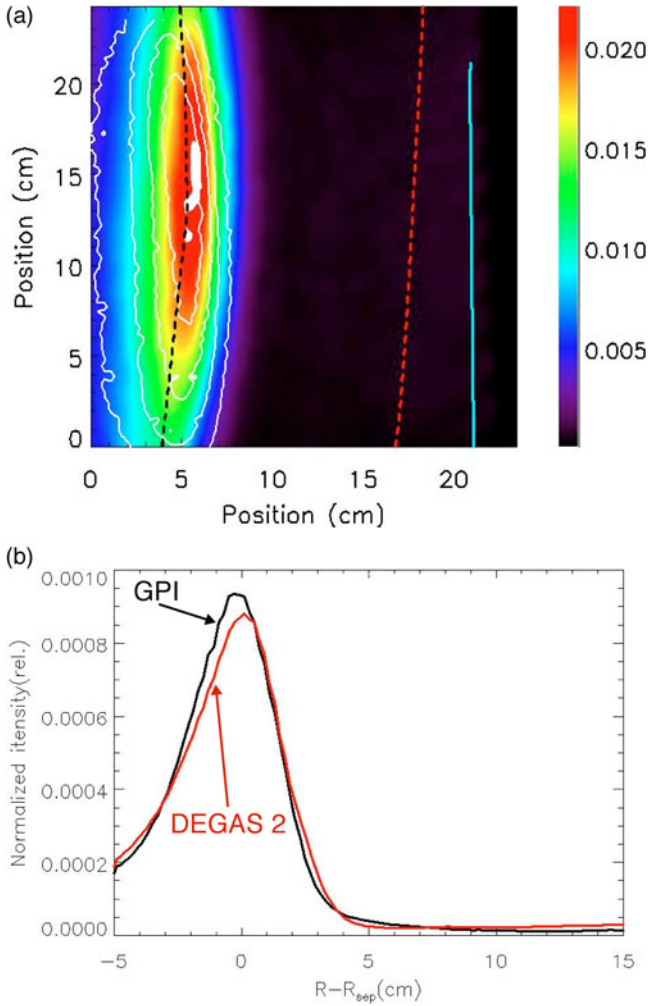


Fig. 7. Comparison between the  $D_\alpha$  light emission from DEGAS 2 and GPI data for #141324. (a) The color contours are the DEGAS 2 results in units of  $W/(sr \cdot m^2)$  (for a gas puff rate of  $8.2 \times 10^{17}$  D atoms per second), the equally spaced white contours are the GPI results, the leftmost dashed line is the separatrix, the rightmost dashed line is the limiter shadow, and the nearly vertical line is the gas manifold. (b) The 1-D profiles are obtained by normalizing the 2-D data to the sum over all pixels and then averaging over vertical pixels. The horizontal coordinate is mapped to the outer midplane separatrix.

temperature profiles at the GPI puff location. These uncertainties could be due to small ( $\sim 1$  cm) variations in the separatrix location during the time of interest, to small-scale turbulent fluctuations seen by the Thomson scattering that are not apparent at the GPI location (e.g., the secondary peak in the DEGAS 2 profile in Fig. 5b at  $R - R_{sep} \approx 5$  cm), or to uncertainties in the mapping of the midplane flux surfaces to the GPI location above the midplane. Thus, the results of Figs. 4 through 7 and Table I can be considered a successful validation of the

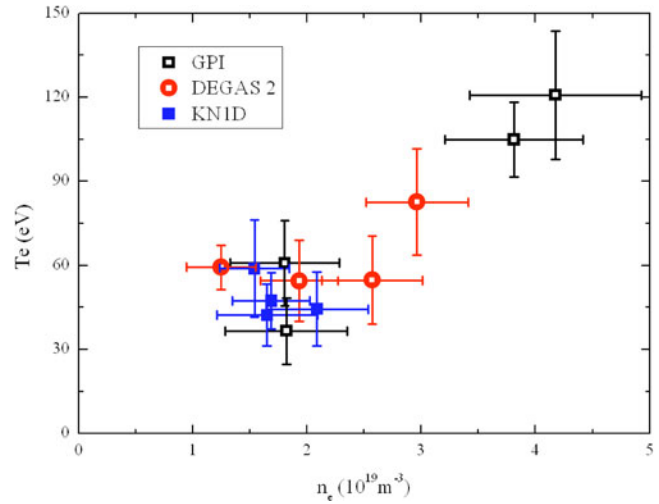


Fig. 8. Electron density and temperature at the peak location of  $D_\alpha$  light from GPI, DEGAS 2, and KN1D. The DEGAS 2 and KN1D modeling used Thomson scattering data as input electron density and temperature profiles and assumed  $T_i = T_e$ . The GPI data are averaged over 10 ms.

DEGAS 2 code with the GPI data, to within the uncertainties of the experimental data.

Figure 8 shows the radial location of the peak of the  $D_\alpha$  light from GPI, DEGAS 2, and KN1D profiles in terms of the local electron density and temperature for the same four shots. The error bars in Fig. 8 are determined by combining a spatial uncertainty of  $\pm 1$  pixel ( $\pm 3$  mm) with (steep) local gradients in electron density (horizontal) and temperature (vertical). The GPI peaks have a wider range in  $T_e$  and  $n_e$  than the DEGAS 2 and KN1D simulations most likely because the GPI signal is affected by fluctuations in the plasma parameters that are not accounted for in these simulations. The two points with the highest  $T_e$  and  $n_e$  at the peak are for shots #141320 and #141322, which also yield the greatest differences in peak width and location when compared with the DEGAS 2 simulations (Table I).

The electron temperatures at the emission peak locations in Fig. 8 are well above the 15 to 18 eV reported for the simulations in Ref. 13, even though those experiments and simulations used a helium gas puff rather than deuterium. That is, one might have expected the helium to penetrate farther (to higher  $T_e$  regions) since its ionization potential of 24.6 eV is well above that for a deuterium atom. But, the initial energy of the deuterium atoms, the  $\sim 3$ -eV Franck-Condon energy obtained from dissociation of the deuterium molecule, is much higher than the room-temperature energy of the helium atoms. Moreover, the deuterium atoms undergo efficient charge exchange with the main plasma ions, resulting in neutral atom temperatures that are a significant fraction of the ion temperature. The combination of these two effects

yields significantly greater penetration for the deuterium atoms.

Finally, it is interesting to compare the radial locations of the peak in the measured  $D_\alpha$  profile with the separatrix locations over longer periods of time, as is shown in Fig. 2. For Fig. 2 the peak in the poloidally averaged GPI light was mapped to the outer midplane using EFIT and then plotted along with the outer midplane separatrix from EFIT. The peak of the  $D_\alpha$  light is almost always within 1 to 2 cm of the separatrix for all times, even for the  $\sim 15$ -ms periods before the GPI puff, except during ELMs when the GPI light suddenly moves outward.<sup>24</sup> This suggests that the comparisons of Figs. 4 through 7 are at least qualitatively similar at other times during these shots and that the GPI gas puff is not significantly perturbing the local plasma parameters during the puff.

#### IV.B. Absolute Magnitude Comparison

We can take the mean number of counts per pixel in the frame, divide by  $\Delta t_i = 2.1 \mu\text{s}$ , and use the calibration factor  $\beta$  from Sec. II to infer the corresponding radiance of the gas puff emission cloud. But, again, we only know the total number of D atoms injected. So, we integrate the camera data in time by summing over all frames recorded during the gas puff and multiplying by the time interval between frames,  $1/397\,660 = 2.5 \mu\text{s}$ . This yields  $\Delta t_{\text{tot}} \bar{c}_p$ , where  $\Delta t_{\text{tot}}$  is the total time interval of the gas puff and  $\bar{c}_p$  is the mean number of counts per frame per pixel. Normalizing this by the exposure time and incorporating the calibration factor, we obtain  $\beta \Delta t_{\text{tot}} \bar{c}_p / \Delta t_i$ , the mean number of photons per pixel emitted during the gas puff per centimeter squared per steradian. Multiplying this by the area of the target plane  $A_{\text{targ}} = 560 \text{ cm}^2$  (i.e., the total number of pixels times the area viewed by a single pixel) and integrating over a total solid angle of  $4\pi$  sr, we finally obtain the total number of photons emitted during the gas puff. For shot #141324,  $\Delta t_{\text{tot}} \bar{c}_p = 4.8 \pm 26\%$  counts  $\cdot$  s per pixel. Incorporating  $\beta = 2.45 \times 10^{14}$  [photons/(sr  $\cdot$  cm<sup>2</sup>  $\cdot$  s)]/[counts/( $\mu\text{s} \cdot$  pixel)] and the other factors,  $4\pi A_{\text{targ}} \beta \Delta t_{\text{tot}} \bar{c}_p / \Delta t_i = 3.94 \times 10^{18}$  photons of  $D_\alpha$ .

The total number of deuterium gas atoms puffed during this shot was measured by the pressure rise in the vessel without a shot (without pumping) and by the drop in pressure in the gas plenum to be  $5.3 \text{ Torr} \cdot \ell$  or  $3.5 \times 10^{20}$  atoms, with an uncertainty of approximately  $\pm 10\%$ . Thus, the absolutely calibrated number of photons emitted per D atom within the GPI field of view in this shot is  $(3.9 \times 10^{18} \text{ photons}) / (3.5 \times 10^{20} \text{ atoms}) \sim 1/89$ , with an uncertainty of approximately  $\pm 34\%$  obtained by combining the calibration error with those from both the photon and the atom measurements.

The DEGAS 2 simulated GPI image of shot #141324 (Fig. 7) provides the radiance for each pixel, e.g., in  $W/(\text{sr} \cdot \text{cm}^2)$ . We can compute a total photon emission

rate in a manner analogous to the above by summing over pixels, dividing by the energy of the  $D_\alpha$  photon, and multiplying by  $4\pi A_{\text{targ}}$ . The end result is  $1.1 \times 10^{16}$  photons/s for a specified total source rate of  $8.2 \times 10^{17}$  D atoms per second, yielding a ratio of 1/75 photons per atom. We estimate the uncertainty in this value as 18%, allowing for variations in the simulation geometry (the sensitivity studies noted above, as well as a few others), different characterizations of the gas puff, and the variations in the assumed plasma profiles. For the last we utilized the standard deviation in the total number of photons in the camera image from the set of 20 variants described in Ref. 13. The experimental and simulated photon-per-atom ratios differ by only  $\sim 20\%$ , well within the overall uncertainty. The relative ratio of GPI to DEGAS 2 light emission for the other three shots (see Table I) were within  $\sim 20\%$  of that for #141324 so that this statement applies to all four shots considered here.

On the other hand, the simulated ratio of 1/75 is considerably smaller than the ratio of 1/15 expected from the atomic physics models.<sup>17,25</sup> The apparent discrepancy can be largely accounted for by two separate factors of 2. First, the emission recorded by the simulated camera represents only about half of the total number of photons. We determine the latter by integrating the volumetric emission rate over the entire simulation volume. Second, roughly half of the puffed atoms exit the simulation (through the vertical boundaries) without emitting photons. The sensitivity test mentioned in Sec. III, in which the vertical boundaries of the problem were expanded by 50%, shows a 14% increase in the total number of photons emitted within the simulation volume. However, the integrated camera signal (its view was not changed) increases by only 3%, demonstrating that the likelihood of exiting neutrals reentering the camera view is small.

#### V. SUMMARY

This paper describes a new validation of the DEGAS 2 Monte Carlo neutral transport code using light emission data obtained with the GPI diagnostic on NSTX. This exercise is new in two ways. First, the absolute magnitude of the light emission is examined, not just the spatial variation. Second, the working gas is deuterium and not helium, as has been used in previous efforts.<sup>13</sup>

The comparison of the simulated and measured light emission spatial profiles is similar to that obtained in that previous effort, with the radial widths and peak locations agreeing to within the estimated uncertainties. Because only the total amount of gas injected by the GPI gas manifold is known, the absolute comparison is made in terms of the total number of photons emitted by the puff and recorded by the GPI camera (as inferred from the absolute calibration of the GPI camera) per injected atom. The experimental result (for a particular plasma discharge)

is  $1/89 \pm 34\%$  photons per atom, while the DEGAS 2 simulation yields  $1/75 \pm 18\%$  photons per atom. The two values thus match to within these uncertainties. One conclusion that we can draw from this is that the relatively simple atomic physics model used to describe the  $D_2$  molecules, ignoring the effects of excited states,<sup>14</sup> is adequate for simulating the relatively high-temperature, low-density plasmas found in the main chamber of NSTX.

With this result, we have confidence that we can apply related techniques to interpret the passive light emission in the NSTX main chamber, via the camera described in Ref. 1, to infer the neutral density profiles in the scrape-off layer and edge plasmas. The neutral sources utilized in these simulations will be ad hoc sources placed at material surfaces in various locations throughout the vacuum vessel. Their relative magnitudes will be calibrated using the measured light emission, allowing us to also learn more about the sources of neutral gas in NSTX.

### ACKNOWLEDGMENTS

The authors wish to thank B. LaBombard of Massachusetts Institute of Technology and B. Davis of Princeton Plasma Physics Laboratory (PPPL) for the help with KN1D, R. J. Maqueda for taking the GPI data used in this experiment, and F. Scotti of PPPL for the help with the calibration of the GPI camera. One of the authors (B. C.) thanks the NSTX team for support during his visit to PPPL. This research was funded by National Nature Science Foundation of China under contract 11021565 and by U.S. Department of Energy contract DE-AC02-09CH11466.

### REFERENCES

1. P. W. ROSS, "Ion Power Balance in Neutral Beam Heated Discharges on the National Spherical Torus Experiment (NSTX)," PhD Thesis, Princeton University (2010).
2. P. HELANDER, T. FULOP, and P. J. CATTO, "Controlling Edge Plasma Rotation Through Poloidally Localized Refueling," *Phys. Plasmas*, **10**, 4396 (2003).
3. R. D. BENGSTON et al., "Measurement of Neutral Density Profile in TEXT Using a Diagnostic Neutral Beam," *Rev. Sci. Instrum.*, **61**, 3110 (1990).
4. R. L. BOIVIN et al., "High Resolution Measurements of Neutral Density and Ionization Rate in the Alcator C-Mod Tokamak," *Rev. Sci. Instrum.*, **72**, 961 (2001).
5. J. HARHAUSEN et al., "Interpretation of  $D_\alpha$  Video Diagnostics Data as a Contribution to Plasma Edge Characterization," *Plasma Phys. Control. Fusion*, **53**, 025002 (2011).
6. R. J. MAQUEDA et al., "Edge Turbulence Measurements in NSTX by Gas Puff Imaging," *Rev. Sci. Instrum.*, **72**, 931 (2001).
7. S. J. ZWEBEN et al., "Edge Turbulence Imaging in the Alcator C-Mod Tokamak," *Phys. Plasmas*, **9**, 1981 (2002).
8. S. J. ZWEBEN et al., "High Speed Imaging of Edge Turbulence in NSTX," *Nucl. Fusion*, **44**, 134 (2004).
9. R. A. PITTS et al., "Status and Physics Basis of the ITER Divertor," *Phys. Scr. T.*, **138**, 014001 (2009).
10. "DEGAS 2 User's Manual": [http://w3.pppl.gov/degas2/Doc/degas2\\_all.pdf](http://w3.pppl.gov/degas2/Doc/degas2_all.pdf) (current as of Mar. 21, 2013).
11. D. P. STOTLER et al., "Neutral Transport Simulations of Gas Puff Imaging Experiments," *J. Nucl. Mater.*, **313–316**, 1066 (2003).
12. D. P. STOTLER et al., "Three-Dimensional Neutral Transport Simulations of Gas Puff Imaging Experiments," *Contrib. Plasma Phys.*, **44**, 294 (2004).
13. D. P. STOTLER et al., "Progress Towards the Validation of Models of the Behavior of Neutral Helium in Gas Puff Imaging Experiments," *J. Nucl. Mater.*, **363–365**, 688 (2007).
14. K. SAWADA and T. FUJIMOTO, "Effective Ionization and Dissociation Rate Coefficients of Molecular Hydrogen in Plasma," *J. Appl. Phys.*, **78**, 2913 (1995).
15. P. T. GREENLAND, "Collisional-Radiative Models with Molecules," *Proc. R. Soc. London, Ser. A*, **457**, 1821 (2001).
16. U. FANTZ et al., "Hydrogen Molecules in the Divertor of ASDEX Upgrade," *J. Nucl. Mater.*, **290–293**, 367 (2001).
17. L. C. JOHNSON and E. HINNOV, "Ionization, Recombination, and Population of Excited Levels in Hydrogen Plasmas," *J. Quant. Spectrosc. Radiat. Transfer*, **13**, 333 (1973).
18. J. C. WEISHEIT, "Recombination in Dense Plasmas," *J. Phys. B*, **8**, 2556 (1975).
19. R. K. JANEV and J. J. SMITH, "Cross Sections for Collision Processes of Hydrogen Atoms with Electrons, Protons, and Multiply Charged Ions," *Atomic and Plasma-Material Interaction Data for Fusion* (supplement to the journal *Nuclear Fusion*), Vol. 4, p. 1 (1993).
20. L. L. LAO et al., "Reconstruction of Current Profile Parameters and Plasma Shapes in Tokamaks," *Nucl. Fusion*, **25**, 1611 (1985).
21. S. A. SABBAGH et al., "Equilibrium Properties of Spherical Torus Plasmas in NSTX," *Nucl. Fusion*, **41**, 1601 (2001).
22. "KN1D: A 1-D Space, 2-D Velocity, Kinetic Transport Algorithm for Atomic and Molecular Hydrogen in an Ionizing Plasma": [http://www.psfc.mit.edu/~labombard/KN1D\\_Source\\_Info.html](http://www.psfc.mit.edu/~labombard/KN1D_Source_Info.html) (current as of Nov. 9, 2012).
23. B. CAO et al., "Edge Turbulence Velocity Changes with Lithium Coating on NSTX," *Plasma Phys. Control. Fusion*, **54**, 112001 (2012).
24. R. J. MAQUEDA, R. MAINGI, and NSTX TEAM, "Primary Edge Localized Mode Filament Structure in the National Spherical Torus Experiment," *Phys. Plasmas*, **16**, 056117 (2009).
25. S. D. LOCH et al., "The Role of Excited State Ionization Data on H and He Generalized Collisional–Radiative Coefficients," *Plasma Phys. Control. Fusion*, **51**, 105006 (2009).